Journal of Information Systems Engineering and Management
2025, 10(55s)
e-ISSN: 2468-4376
https://www.jisem-journal.com/

Research Article

Vessels Detection in Complex Coastal Area using Hybrid CNN Inspired Dense Connected Model

Kritika Vaid[1], Dr. Ravinder Singh Madhan[2]
[1]*Research Scholar, Department of Computer Science & Engineering, IEC University, Baddi-174103, Solan, Himachal Pradesh, India*
kritikavaid172@gmail.com
[2]*Research Guide and Associate Professor, Department of Computer Science & Engineering, IEC University, Baddi-174103, Solan, Himachal Pradesh, India*
ravimadhan@gmail.com

ARTICLE INFO

Received: 14 Jun 2025

Revised: 16 Jun 2025

Accepted: 18 Jun 2025

ABSTRACT

In this work, we propose a practical and efficient approach for ship detection in remote sensing images.Themethod combines body and ship wake detection by combining deep learning and feature-based visual processing.A deep convolutional neural network (CNN) is used to accurately identify ship bodies, while a feature-driven processing method is developed to detect ship wakes.To enhance analysis, we model the sea area and assess image quality.Duetothe backdrop features like clouds and ocean foam, make it hard to find the actual target ship, it is usually quite difficult to recognize ships in a crowded setting.The suggested process is used to first separate the backdrop from the aim, whereas previous methods were limited to locations with clear conditions.Wake detection is crucial for determining sailing orientation and aiding ship recognition.Notably, it makes it possible to identify ships that are outside the picture limits or obscured by clouds with some awareness.To solve the challenges of identifying ships in crowded backgrounds, a CNN-based model trained on large-scale remote sensing datasets is used.The system is optimized using sophisticated data augmentation approaches to improve generalization over a range of marine environments.A multi-scale feature extraction technique is also incorporated to enhance the detection of ships with varying sizes and orientations. Theproposed method is effective, as demonstrated by experiments on real remote sensing datasets, with identification rates of over 70% for targets.

Keywords: Ocean engineering, wake detection, image processing, vessel tracking, and remote sensing.

I. INTRODUCTION

Applications for automatically detecting sailing ships are many in both the commercial and marine domains [1]. Ocean surveillance relies heavily on remote sensing due to its high resolution and broad field of view [2], when the target's "Automatic Identification System (AIS)" is disabled. Remote sensing imagery has been classified into two types based on the sensing payload: SAR images and visible images [3-5]. Unlike passive sensors including optical and infrared sensors, SAR actively emits microwaves for observation without affected by climatic factors such as temperature, light and clouds [6-7]. These benefits allow SAR to conduct earth exploration activities that are stable throughout the long term, day and night. Distribution model method of sea background [8-10] and the detector designing methods [11-13] are the most concerned aspects in CFAR.

To enhance the detection performance in SAR images, the image segmentation technique is also employed [14].

Finding additional attributes is crucial when the ship body's characteristics are hidden in a picture. Ship sailing may produce wakes that span a wide region of the sea surface and linger for a very long period [15]. Consequently, ship ripples have a higher monitoring chance than the ship body and their detection features are more evident than the object of investigation itself. Additionally, it is possible to forecast the target's exact quickly, course, and real position more precisely by merging its aftermath with the the audience's place within the picture.

Traditional methods use linear features in SAR images of ship wakes [16].A visible distant recognising image has an increased objective and may gather greater amounts of local information, which makes the results more useful for comprehension and additional research. In comparison with SAR, a visible image has the advantages of vision and low

Journal of Information Systems Engineering and Management
2025, 10(55s)
e-ISSN: 2468-4376
https://www.jisem-journal.com/

Research Article

cost. Customary discovery techniques typically based on visual saliency and visual discernment principles, the Itti [29] model, Ft [30] model, SR [31] model, AC [32] model, and GBVS [33] model are broadly utilized in extricating transport locales from the ocean foundation. Furthermore, the Histogram of the Situated Angle (Hoard) descriptor is ordinarily involved in highlighting descriptors in transport discovery [34]. By and large, these above conventional calculations have unsuitable location execution under a complex foundation environment. The convolutional brain organization (CNN) based technique is particularly compelling in transport identification of noticeable remote detecting pictures. Profound learning strategies can successfully conquer the weaknesses of human plans, and because of the huge limit of the model, the objective can be depicted exhaustively, which incredibly works on the exactness of identification. As indicated by their handling steps, profound learning organization can be partitioned into a two-stage recognition technique and a single-stage location strategy. Two-stage recognition strategy is done with the construction of conventional techniques, the entire picture is navigated to produce a few competitor boxes, and afterward the up-and-comer boxes are ordered to decide if there is an objective nearby and afterward network is utilized to fine-find and group the objective. “R-CNN” [35], “Quick R-CNN” [36], and “Veil R-CNN” [37] are the normally utilized systems. Single-stage location strategy is proposed to anticipate various jumping boxes and class probabilities for these cases at the same time in one assessment. You just look once (Consequences be damned) [38-39] is perhaps of the most agent technique that can perform constant identification with fewer bogus positive discoveries on the foundation.

Since there are few research on the analysis of ship wakes in apparent from satellite photographs, these proposed strategies focus on the identification of ship bodies. As previously stated, outside variables can influence visible remote sensing images, thus waves can be used to aid in boat location.

In contrast, the ship seems to have distinct local characteristics in superior resolution visible remote sensing photos and is shown as an area with a particular form rather than a fine-line segment. Because of this, visible remote sensing pictures are challenging to handle using conventional SAR image processing techniques.

II. RELATED WORK

The authors [1-4] introduced a novel method, based on the analysis of “synthetic aperture radar” (SAR) data, which is f requently utilized for ship identification & monitoring.Their study fared effectively across multiple locations, according to the results of testing the proposed method using a sizable public SAR ship identification collection. The correctness of the suggested model was 92.8 per cent along with 92.7%, with both dense and non-dense links. The authors of [5-8] investigated deep learning frameworks for synthetic aperture radar ship detection methods. The proposed technique [9-15] with its image dataset achieved an accuracy of 79.8%. This study uses a network of on-land security cameras to create an immediate detection technique.

Dueto so many different ship models, traditional “convolution neural network (CNN)” techniques are laborious and im precise. Noticing the ship type and position using CNN, this model corrects the location by applying global contrast-based salient region detection [16].

A dataset of optical remote-sensing images with high-resolution was used to test the method's accuracy and validity [17–23]. The proposed technique reduced the time of computation in comparison to computational time of all available detection methods [24].“ Discriminative features of inclined candidate areas for ship classification were extracted by using a rotating region of interest pooling layer [25-28]. With the use of a rotating ship dataset and the HRSD2016 benchmark, they demonstrated that their suggested solution exceeds existing best practices in arbitrary-oriented ship recognition [29].They introduced an altered Fisher metric framework built around knowledge geometry by combining the lognormal method with Riemannian geometry”. As per tests performed by the authors [30-35], “Lognormal metrics for SAR images” may be modified to improve contrast between object and background and reduce false alarm rates for ship recognition.

III. PROPOSED Method (SHIP DETECTION)

Figure 1 shows the generalized ship detection method steps. The ability to identify findings are limited by the sea segment inquiry, which separates the sea region from the satellite photographs and assesses the picture sharpness. Next, we carry out ship wake along with ship body detection in turn, and we assess the detection outcome.

Journal of Information Systems Engineering and Management
2025, 10(55s)
e-ISSN: 2468-4376
https://www.jisem-journal.com/

Research Article

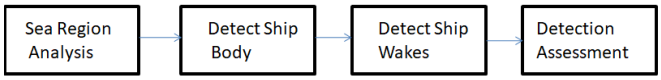

Figure 1: Ship Detection Process

3.1 Sea-region analysis

Gauss filter with a minimal variance has been apply to de-noise the initial remote-sensing picture. The following steps are required for the analysis of the sea region.

Step1: Remove the Sea Area.

In order to have an effective colour opposition, the image from the RGB colour system has been converted to the LAB colour space since the sea region in an accessible photograph often has a hue that is close to blue. The marine region's mean value, shown by the A and B values, is obtained by combining a number of separately taken images.
Following clustering, we fill in the gaps and eliminate snowflakes from the retrieved ocean region by performing morphological opening and closure. Based on the linked component analysis's outcome, mark the area of interest.

Step2: Mark the area of clouds in the sea area

The cloud cover obscures the object in remote sensing images. The cloud region has been identify using the previously used dark channel [43]. The dark channel of a picture can be identified by:

$$J^{dark}(x1) = \min_{c\in\{r,g,b\}} \left(\min_{y\in\Omega(x1)} J^{c}(y) \right) \qquad (1)$$

Here, "J^c is the color channel of the remote sensing image" and "$\Omega(x1)$ is a local patch centered at x1". The shadow channel of a picture has a value around 0, with the exception of the hazy region.

We initially select the first 0.1 percent, of the black multiple channels image's pixels in intensity attempt as the cloud pixels to attempt to recognize the cloud area. In that order, we afterwards does connected analysis of components, structural launching along with morphological shutting.

Step3: Image Quality Evaluation

The ocean part of the image is only taken into account. The ocean background C_{bg} is the different set of ocean regions C_{sea} and cloud region C_{cloud}:

$$C_{bg} = C_{sea} - C_{cloud} \qquad (2)$$

Fig 2(a): Different Ships

Journal of Information Systems Engineering and Management
2025, 10(55s)
e-ISSN: 2468-4376
https://www.jisem-journal.com/

Research Article

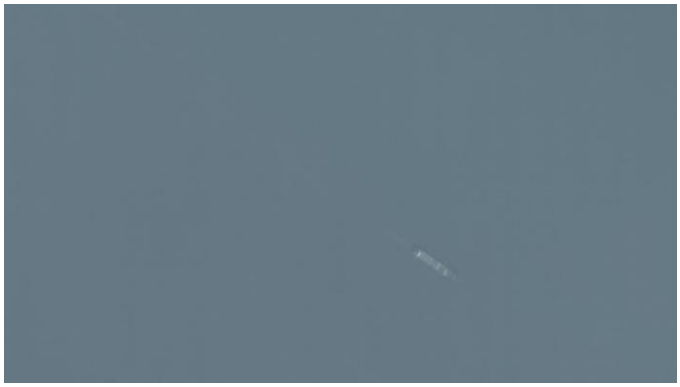

Fig 2(b): Background of Environment

In order to describe the picture quality, we offer an extra criterion for quantitative assessment:

$$QI = \prod_{i=1}^{n} I_i^{\frac{w_i}{n}}, QI \in [0,1] \quad (3)$$

Better quality in images is indicated by a greater value. Here, the weight of the related indication is used to reflect the normalised indication produced by the image's description.

The characteristics image "entropyH_e" [44], "Tenengrad gradientH_T" [45], "Gabor featureH_G" and "reblur performance H_R" are used to calculate the image quality in this work.

The image entropy H_e is computed as:

$$H_e = -\sum(p \times log_2(p)) \quad (4)$$

Where a higher number denotes higher resolution. It comprises the image's normalized histogram values.
This is how the T enengrad inclination is calculated:

$$H_T = \sum(G_x^2(x,y) + G_y^2(x,y)) \quad (5)$$

Where "$G_x(x,y), G_y(x,y)$" represents, accordingly, the directional gradation in both the horizontal and vertical dimensions; a higher value denotes higher-quality images.

A common linear bandpass filter in image processing, the Gabor filter is used for disparity estimation, texture categori zation, edge detection, and feature extraction [46]. The "Gabor feature H_G" is the maximum image entropy of the "response matrix $\{R_G\}$" obtained by convolving the original image Im_0 with the "Gabor filters $\{g(x,y|\lambda,\theta,\psi,\sigma,\gamma)\}$":

$$g(x,y|\lambda,\theta,\psi,\sigma,\gamma) = exp(-\frac{\tilde{x}^2+\gamma^2\tilde{y}^2}{2\sigma^2}) exp\left[i\left(2\pi\frac{\tilde{x}}{\lambda}+\psi\right)\right],$$
$$\tilde{x} = x\cos\theta + y\sin\theta, \tilde{y} = -x\sin\theta + y\cos\theta \quad (6)$$

and

$$R_G = g(x,y|\lambda,\theta,\psi,\sigma,\gamma) * Im_0$$
$$H_G = max(H_e(\{R_G\})) \quad (7)$$

Here, orientations $\theta = [0, \frac{\pi}{6}, \frac{\pi}{3}, \frac{\pi}{2}, \frac{2\pi}{3}, \frac{5\pi}{6}]$ and wavelength $\lambda = [2,4,8]$, and a larger value H_G indicates "better image quality".

" Here, $Im' = G_f(\sigma) * Im_0$ is the blurred image using a Gaussian filter G_f with a variance of σ;$SSIM()$is the Structure Similarity Index Measure (SSIM) to measure the similarity between two images from the same capture, which is based on the idea that the human visual system is sensitive to structural information in the scenes" [48]:

$$SSIM(Im', Im_0) = [l(Im', Im_0)]^{\alpha} \cdot [c(Im', Im_0)]^{\beta} \cdot [s(Im', Im_0)]^{\gamma}$$
$$l(Im', Im_0) = \frac{2\mu_x\mu_y+C_1}{\mu_x^2+\mu_y^2+C_1}, c(Im', Im_0) = \frac{2\sigma_x\sigma_y+C_2}{\sigma_x^2+\sigma_y^2+C_2}, s(Im', Im_0) = \frac{\sigma_{xy}+C_3}{\sigma_x\sigma_y+C_3} \quad (9)$$

Journal of Information Systems Engineering and Management
2025, 10(55s)
e-ISSN: 2468-4376
https://www.jisem-journal.com/

Research Article

Where $\sigma_x, \sigma_y, \mu_x, \mu_y, \sigma_{xy}$denotes the "standard deviations", "local means", and "cross-covariance" for images Im_0 and Im' ; C_1, C_2, C_3 arethe small regularization constants; α, β, γ are the "weighting coefficients". The value of H_R approximately equal to 0 signifies the better image quality.

$I_i(i-1,2,3,4)$ are calculated as:

$$I_1 = (1 + exp(a_1(H_e - b_1)))^{-1}, I_2 = (1 + exp(a_2(H_T - b_2)))^{-1}$$
$$I_3 = (1 + exp(a_3(H_G - b_3)))^{-1}, I_4 = 1 - (1 + exp(a_4(H_R - b_4)))^{-1} \quad (10)$$

Where a_i, b_i $(i = 1,2,3,4)$are the parameters.

Table 2 displays the achievement of various metrics. We can ascertain the overall certainty of recognition and the next operation process based on the.

Step4: Ocean background Modeling

"Here, we convert the ocean background to standardized grayscale and use the Burr type XII distribution [49] to model the ocean background, since we find the background distribution has a unimodal form and is skewed to the right (as seen in Fig. 9)".

$$F(x|\alpha, c, k) = 1 - \frac{1}{(1 + (x/\alpha)^c)^k}$$
$$f(x|\alpha, c, k) = \frac{kc}{\alpha}\left(\frac{x}{\alpha}\right)^{c-1}\left(1 + \frac{x}{\alpha}\right)^{-k-1} \quad (11)$$

where, $\alpha, c, k > 0$ are the distribution parameters.

3.2 Ship Body Detection

The goal of the ship body detection challenge is to find examples of ships that exhibit a particular trait. Both a classification and a localization operation are included. The ship area usually occupies very little space in an inaccurate sensing image. For example, the ship usually takes up barely any space and is less than 200200, whereas the photographs that are used are usually 19201080. It is challenging for conventional methods to get sufficient results because of the small items.

In the past few decades, deep learning has shown great potential in handling images, which is broadly used in the recognition of objects. The full detection process is implemented on a single network via the one-stage immediate time recognition of objects technique known as YOLO. Ship hulls may be identified in data from satellite imaging by using the YOLO (You Only Look Once) model's current object recognition capabilities. It processes the entire image in a single neural network run, simultaneously predicting limit boxes along with the likelihood of classes.

YOLO learns to differentiate ship structures from the

surrounding sea debris by using annotated ship hull datasets. Its multi-scale feature extraction ensures resilience in a range of environmental situations by enabling the identification of hulls of diverse sizes and orientations.

To detect the ship body, we train a YOLOv5 network [22] with one category using the dataset [50] with picture enhanc ement.We further verify the YOLO identification zone by relaxing it to twice its side lengths and retaining just those

Journal of Information Systems Engineering and Management
2025, 10(55s)
e-ISSN: 2468-4376
https://www.jisem-journal.com/

Research Article

relaxed portions where over fifty per cent of the area is ocean backdrop.C_{bg}.Over 90% of ship bodies may be detected with precision.

3.3 Ship Wakes Detection

We now go over our wake detection technique and its range of use. The following stages are often included in the wake detection approach. We see that only these photos are deemed significant for wake extraction if their quality value is more than the clear threshold.

Step 1:Determine the wake-searching region

Based on various usage objectives, the wake-searching area$S_r$comprises three types: the community of the ship bodyS_1, The border region and the cloud neighbourhoodS_3.

We utilise the method of principle component analysis (PCA) to determine the ship direction because the shipping has a significant length-width ratio and the ship body neighbourhood is located along an axis of the vessel detection window:

$$S\frac{1}{n-1}\sum_{i=1}^{n}(\boldsymbol{x}_i-\boldsymbol{\mu})(\boldsymbol{x}_i-\boldsymbol{\mu})^T \quad cov$$

$$S\sum_{i=1}^{d}\lambda_i\boldsymbol{v}_i\boldsymbol{v}_i^T\sum_{i=1}^{k}\lambda_i\boldsymbol{v}_i\boldsymbol{v}_i^T \quad cov \tag{12}$$

Here, we organize the vessel sector as well as is the vessel region placement matrix's covariance matrix;

$\lambda_i, \mathrm{v_i}$is the appropriate eigenvectors and the eigenvalues sorted from big to small; for an a two-dimensional picture,

$k = d = 2$ and $\boldsymbol{v}_1, \boldsymbol{v}_2$are the long and short axis directions of the vessel, respectively.

The $S_1$is produced using the binarized vessel area's minimal bounding rectangle, which has four times its length.

The cloud neighborhood is created using the cloud region's smallest boundary rectangle.

"$C_{cloud}$with around 50–100 meters between them. There are additional 50–100 m buffers around the border area".

Step 2: The turbulent wake search in S_r

The turbulent wake and the Kelvin wake are among the more frequently seen wake forms in satellite photos as shown in Figure 1.The turbulent wake often exhibits a bigger size and a more concentrated distribution of grey scale than the Kelvin wake. In this study, we identify the turbulent wake to aid in ship detection since these make the detection of turbulent wake more reliable.

We start by converting the picture from RGB space to LAB space for every wake-searching region that was acquired in Step 1. The "Burr type XII distribution's log-likelihood" function is:

$$log(L_B) = -(k+1)\sum_{i=1}^{n} log\left(\left(\frac{x_i}{\alpha}\right)^c + 1\right) + (c-1)\sum_{i=1}^{n} log(x_i) - cn\,log(\alpha) + n\,log(c) + n\,log(k) \tag{13}$$

To determine the parameters, we employ the maximum likelihood estimation (MLE) technique. However, because non-degenerated limiting distributions may exist, finite maximum likelihood estimates for the Burr type XII distribution are not always available [51]. When the Burr type XII distribution cannot be solved, we employ the Gamma distribution as a substitute distribution form. The Gamma distribution's cdf and pdf are:

Journal of Information Systems Engineering and Management
2025, 10(55s)
e-ISSN: 2468-4376
https://www.jisem-journal.com/

Research Article

$$f_G(x|L,\mu) = \left(\frac{L}{\mu}\right)^L \frac{x^{L-1}e^{-Lx/\mu}}{\Gamma(L)}, F_G(x|L,\mu) = \frac{1}{\Gamma(L)}\int_0^{Lx/\mu} t^{L-1}e^{-t}\,dt \quad (14)$$

where $x, L, \mu > 0$; and the Gamma function $\Gamma(a)$ is $\Gamma(a) = \int_0^{+\infty} t^{a-1}e^t dt$.
The MLE of Gamma distribution parameters is:

$$\hat{\mu} = \frac{1}{n}\sum_{i=1}^{n} x_i, \frac{d(ln(\Gamma(L)))}{dL} = ln\left(\frac{L}{\hat{\mu}}\right) + \frac{1}{n}\sum_{i=1}^{n} ln\, x_i \quad (15)$$

IV. RESULTS AND DISCUSSIONS

The methods evaluated in the previous section are demonstrated in the "AIR-MOT dataset" [53]. We use the high-resolution, large-scale "Jilin1 satellite video dataset" for multi-object tracking, filtering out more than 1,000 photos of ships in motion and 200 opposing views of the ocean devoid of ships. These data help us assess our approach. The "AIR-MOT" dataset is suggested for tracking objects, and even in cases when the goals are not viewable in a particular image, additional measurements can assist in determining the actual ship position.

In remote sensing, ship detection refers to the use of satellite or aerial imagery to locate and identify ships in maritime environments. By learning hierarchical spatial characteristics and differentiating ships from sea debris, deep learning techniques like "Convolutional Neural Networks (CNNs)", "You Only Look Once (YOLO)", and "Faster R-CNN" improve accuracy. By concentrating on pertinent areas of the image and disregarding noise, transformer-based models and attention mechanisms enhance detection even more. To improve robustness, deep learning can be combined with feature-based techniques like spectral analysis and wake detection. These methods provide accurate ship detection even in difficult circumstances, making them essential for maritime surveillance, defence, and environmental monitoring applications.

4.1Sea-region separation

First, we exhibit the sea-region separation that results; the extracted sea region is represented by the white pixels, and Figure 3 displays the matching original remote sensing pictures.The outcome shows that the technique can separate sea regions quickly, effectively, and adaptively, which can be used to restrict the detection region.

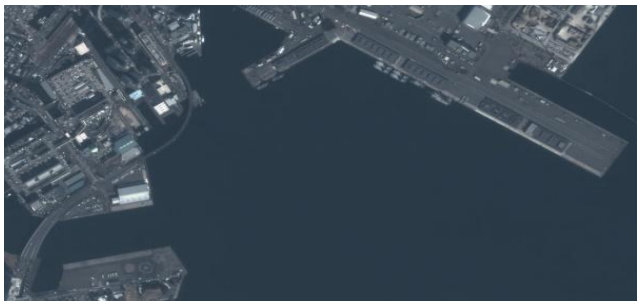

(a)

Journal of Information Systems Engineering and Management
2025, 10(55s)
e-ISSN: 2468-4376
https://www.jisem-journal.com/

Research Article

(b)

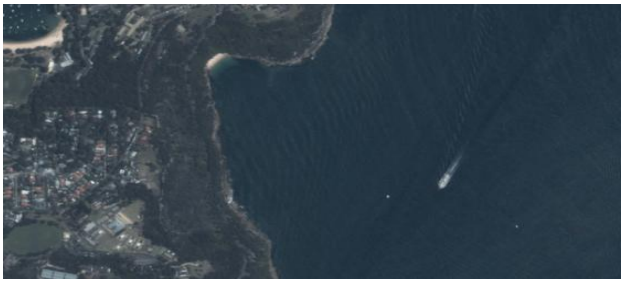

(c)

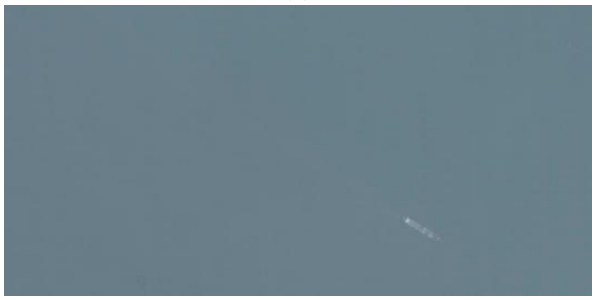

(d)

Figure 3: The original remote-sensing images

(a)

(b)

Journal of Information Systems Engineering and Management
2025, 10(55s)
e-ISSN: 2468-4376
https://www.jisem-journal.com/

Research Article

(c)

(d)

Figure 4: The performance of sea-region separation

The cloud detection performance is displayed, along with the original remote sensing image and the cloud recognition result. The recovered cloud area is indicated by the white pixels, and the average computation time is approximately 2.90 seconds. It is evident that the detection process can offer a suitable segmentation for additional processing.

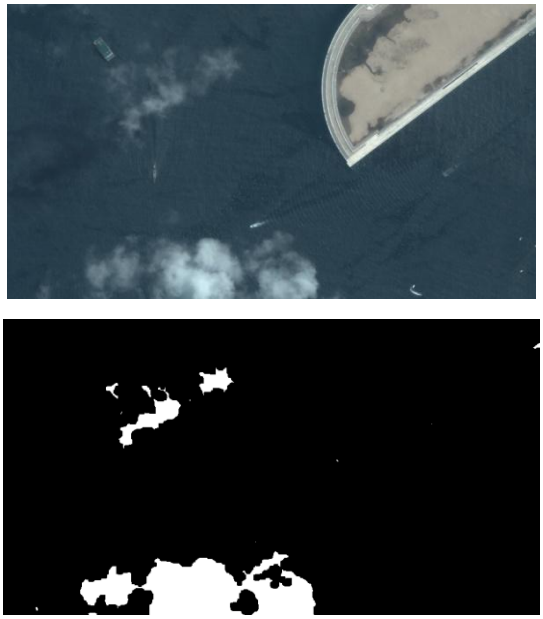

Figure 5: The performance of cloud detection

4.2 Sea Background Analysis

The cloud detection performance is displayed, along with the original remote sensing image and the cloud recognition result. The recovered cloud area is indicated by the white pixels, and the average computation time is approximately 2.90 seconds. It is evident that the detection process can offer a suitable segmentation for additional processing.

Journal of Information Systems Engineering and Management
2025, 10(55s)
e-ISSN: 2468-4376
https://www.jisem-journal.com/

Research Article

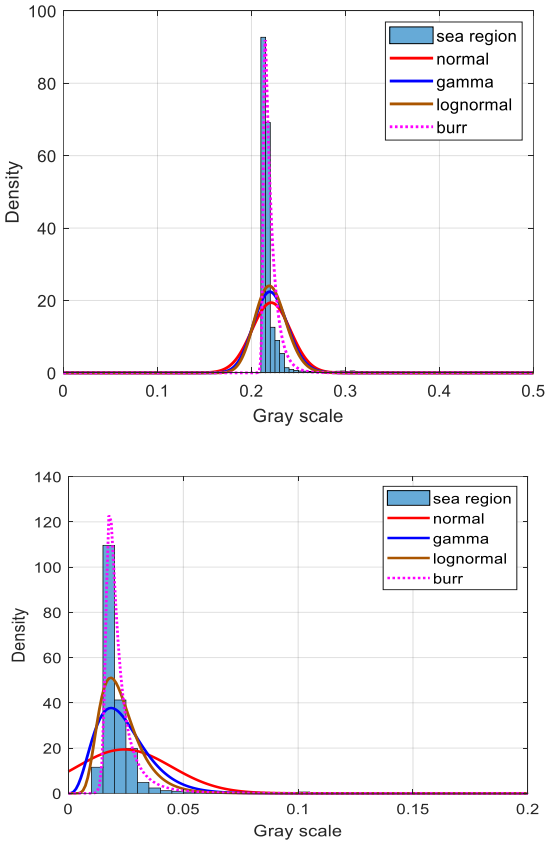

Figure 6: The modeling performance in original grayscale (a) and the standardized grayscale (b)

The results of fitting dispersion curves as well as the L-value histogram of every model we employed to depict the sea background of the images in Figure 6 are shown in Figure 10..

Since the Burr type XII distribution has the smallest average as well as variance KLD when contrasted to the real dispersion, it is evident that it has the best forecasting ability. Additionally, we observe that the Gamma distributed patterns have lower KLD for higher quality images; for this cause, we choose the Gamma distribution as another distribution.

Table 1

KLD of Different Methods

	Normal	Gamma	Lognormal	Burr type XII
Image (a)	2.2350	0.9067	0.4849	0.2664
Image (b)	1.2977	0.1998	0.1340	0.2028
Image (c)	0.0437	0.0250	0.0753	0.0157
Image (d)	0.0697	0.0439	0.0513	0.0561

Journal of Information Systems Engineering and Management
2025, 10(55s)
e-ISSN: 2468-4376
https://www.jisem-journal.com/

Research Article

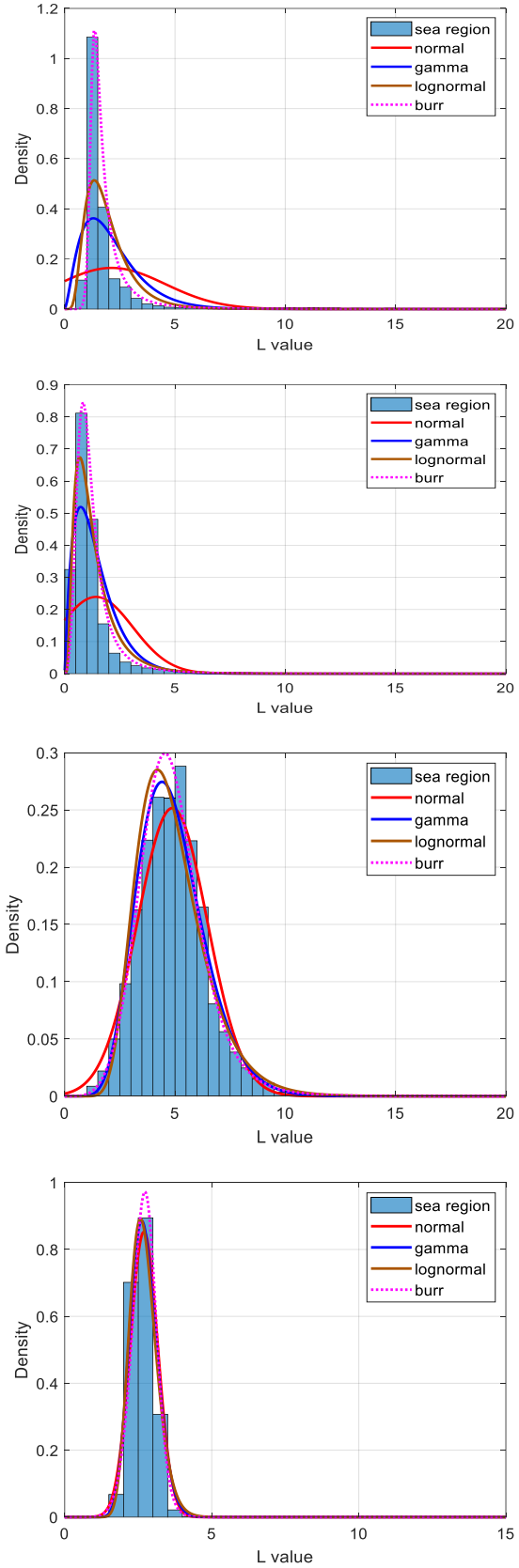

Figure 7: The performance of sea background modeling

Journal of Information Systems Engineering and Management
2025, 10(55s)
e-ISSN: 2468-4376
https://www.jisem-journal.com/

Research Article

Table 2

Performance of image quality indicators

	H_e	H_T	H_G	H_R	QI	Intuition
Fig .6 (a)	2.3050	21.5425	4.7419	0.9841	0.8836	common
Fig .6 (b)	2.5348	12.9861	5.6017	0.9679	0.9296	common
Fig .6 (c)	3.8685	50.5564	7.3810	0.9660	0.9870	good
Fig .6 (d)	2.1113	2.9499	5.4744	0.9971	0.1669	bad
Fig. 11(a)	5.4253	90.8874	7.2396	0.9701	0.9890	good
Fig. 11(b)	3.7863	79.6189	7.3615	0.9607	0.9865	good

Ship Detection Proposed Approach Results

Model	IoU	mAP	ore carrier	bulk cargo carrier	general cargo ship	container ship	fishing boat	passenger ship	FPS (Titan Xp)
YOLOv2+FT[36]	0.7133	0.835	0.840	0.850	0.880	0.888	0.768	0.781	1.5
YOLOv2+SEG[37]	0.7217	0.841	0.840	0.850	0.881	0.888	0.735	0.853	3
YOLOv2+CA[38]	0.7162	0.839	0.841	0.857	0.880	0.888	0.742	0.828	0.3
YOLOv2+GC[39]	0.7309	0.862	0.872	0.870	0.902	**0.907**	0.781	**0.888**	40
YOLOv2	0.7069	0.830	0.849	0.850	0.881	0.888	0.733	0.781	**83**
Ours	**0.7453**	**0.874**	**0.881**	**0.876**	**0.917**	0.903	**0.783**	0.886	49

V. CONCLUSION

This study combines the advantages of feature-based image processing with deep convolutional neural networks to provide a workable and efficient technique for identifying ships in visible remote sensing photos. The wake detection method is utilised in many places, and our approach uses a YOLOv5 network to identify ship bodies quickly and accurately. To evaluate the condition and quality of the sea region, a sea-region analysis approach is suggested. We suggested a reliable wake-based ship detection technique for the difficult cloud coverage and image border region, where ships are usually not visible in a remote sensing picture. The Burr type XII distribution is used to model the extracted sea region, and the modelled sea distribution is used to identify ship wakes.

REFERENCES

[1] S. K. Chaturvedi, “Study of synthetic aperture radar and automatic identification system for ship target detection,” J. Ocean Eng. Sci., vol. 4, no. 2, pp. 173–182, Jun. 2019.
[2] Shi H, He G, Feng P, et al. "An On-Orbit Ship Detection and Classification Algorithm for Sar Satellite." IGARSS 2019 - 2019 IEEE International Geoscience and Remote Sensing Symposium IEEE, 2019.
[3] B, Miaohui Zhang A, et al. "Phase spectrum based automatic ship detection in synthetic aperture radar images - ScienceDirect." Journal of Ocean Engineering and Science (2020).
[4] Copeland, A. C., G. Ravichandran and M. M. Trivedi, "Localized Radon transform-based detection of ship wakes in SAR images." IEEE Trans Grs 33.1(1995):35-45.
[5] Tello, M., C. Lopez-Martinez, and J. J. Mallorqui, "A Novel Algorithm for Ship Detection in SAR Imagery Based on the Wavelet Transform." IEEE Geoscience & Remote Sensing Letters 2.2(2005):201-205.
[6] Song, Chong Jin, and Z. M. Hui, "Survey of the Study on Ship and Wake Detection in SAR Imagery." Acta Electronica Sinica (2003).

[7] Gahfarrokhi J K, Abolghasemi M. Fast VI-CFAR Ship Detection in HR SAR Data[C]. 2020 28th Iranian Conference on Electrical Engineering (ICEE). 2020: 1-5.
[8] Gao G. Statistical modeling of SAR images: a survey[J]. Sensors (Basel). 2010, 10(1): 775-795.
[9] Ao W, Xu F F.,"Robust ship detection in SAR images from complex background," IEEE International Conference on Computational Electromagnetics, 2018: 1-2.
[10] Ai J, Yang X, Song J. An adaptively truncated clutter-statistics-based two-parameter CFAR detector in SAR imagery[J]. IEEE Journal of Oceanic Engineering, 2018, 43(1): 267-279.
[11] Smith M E, Varshney P K. VI-CFAR: A novel CFAR algorithm based on data variability[C]. Radar Conference, 1997, 263-268.
[12] Jin, Yuanwei, and B. Friedlander, "A CFAR adaptive subspace detector for second-order Gaussian signals." IEEE Transactions on Signal Processing 53.3(2005):871-884.
[13] Zhang, Renli, W. Sheng, and X. Ma, "Improved switching CFAR detector for non-homogeneous environments." Signal Processing 93.1(2013):35-48.
[14] Zhai L, Li Y, Su Y. "Segmentation-based ship detection in harbor for SAR images," 2016 CIE International Conference on Radar (RADAR). IEEE, 2017: 362-366.
[15] Hennings I, Romeiser R, Alpers W. Radar imaging of Kelvin arms of ship wakes[J]. International Journal of Remote Sensing, 1999, 20(13): 2519-2543.
[16] Yang T, Karaku O, Achim A,"Detection of Ship Wakes in SAR Imagery Using Cauchy Regularisation," 2020 IEEE International Conference on Image Processing (ICIP). 2020, 3473-3477.
[17] Ballard, D. H., "Generalizing the Hough transform to detect arbitrary shapes." Pattern Recognition 13.2(1981):111-122.
[18] Beylkin, G., "Imaging of discontinuities in the inverse scattering problem by inversion of a generalized Radon transform." Journal of Mathematical Physics 26.1(1985).
[19] Rey M. T., Tunaley J. K., Folinsbee J. T. Application of Radon transform techniques to wake detection in SEASAT-A SAR Images[J]. IEEE Transactions on Geoscience & Remote Sensing, 1990, 28(4): 553-560.
[20] Mata M D, Jarabo A P, Jimenez C B. "Application of mean-shift filtering to ship wakes detection in SAR images," Synthetic Aperture Radar (EUSAR), 2010 8th European Conference on. VDE, 2010: 230-234.
[21] Biondi F. A polarimetric extension of low-rank plus sparse decomposition and Radon transform for ship wake detection in Synthetic Aperture Radar images[J]. IEEE Geoscience &Remote Sensing Letters, 2019, 16(1): 75-79.
[22] Biondi F. Low-rank plus sparse decomposition and localized Radon transform for ship-wake detection in Synthetic Aperture Radar images[J]. IEEE Geoscience & Remote Sensing Letters, 2018, (1): 1-5.
[23] Graziano M D. "SAR-based ship route estimation by wake components detection and classification," 2015 IEEE International Geoscience and Remote Sensing Symposium (IGARSS), 2015: 3255-3258.
[24] Copeland A. C., Ravichandran G, Trivedi M. M. Localized Radon transform based detection of ship wakes in SAR images[J]. IEEE Transactions on Geoscience & Remote Sensing, 1995, 33(1): 35-45.
[25] Chen P, Li X. Zheng G. "Rapid detection to long ship wake in synthetic aperture radar satellite imagery," Journal of Oceanology & Limnology, 2019, 37: 1523- 1532.
[26] K. Zhao, Y. Zhou and X. Chen, "A Dense Connection Based SAR Ship Detection network," 2020 IEEE 9th Joint International Information Technology and Artificial Intelligence Conference (ITAIC), Chongqing, China, 2020, pp. 669-673.
[27] R. Wang et al., "An Improved Faster R-CNN Based on MSER Decision Criterion for SAR Image Ship Detection in Harbor," IGARSS 2019 - 2019 IEEE International Geoscience and Remote Sensing Symposium, Yokohama, Japan, 2019, pp. 1322-1325.
[28] B. Kim, M. Yoo and S. Kim, "SAR Ship Detection with Deep Land Detection Networks and Land Masking," 2022 IEEE International Conference on Consumer Electronics-Asia (ICCE-Asia), Yeosu, Korea, Republic of, 2022, pp. 1-3.
[29] Itti L, "A model of saliency-based visual attention for rapid scene analysis," IEEE Trans, 1998, 20.
[30] R Achanta, S Hemami, F Estrada, et al. "Frequency-tuned salient region detection," IEEE, 2009.
[31] HOU X, ZHANG L. "Saliency Detection: A Spectral Residual Approach," IEEE Conference on Computer Vision & Pattern Recognition. IEEE, 2007.

[32] Achanta R, Estrada F, Wils P, et al. “Salient Region Detection and Segmentation,” computer vision systems; ICVS 2008.
[33] B Schölkopf, Platt J, Hofmann T, Graph-Based Visual Saliency. MIT Press, 2007.
[34] S. Qi, J. Ma, J. Lin, Y. Li and J. Tian, "Unsupervised Ship Detection Based on Saliency and S-HOG Descriptor from Optical Satellite Images," in IEEE Geoscience and Remote Sensing Letters, vol. 12, no. 7, pp. 1451-1455, July 2015.
[35] Zhang, Ning, et al. "Part-based R-CNNs for Fine-grained Category Detection." Springer International Publishing (2014).
[36] R. Girshick and Ieee, "Fast R-CNN," in IEEE International Conference on Computer Vision, Santiago, CHILE, Dec 11-18 2015, in IEEE International Conference on Computer Vision, 2015, pp. 1440-1448.
[37] He, Kaiming, et al. "Mask R-CNN." IEEE Transactions on Pattern Analysis & Machine Intelligence (2017).
[38] J. Redmon, S. Divvala, R. Girshick, and A. Farhadi, "You Only Look Once: Unified, Real-Time Object Detection," in 2016 IEEE Conference on Computer Vision and Pattern Recognition (CVPR), 27-30 June 2016 2016, pp. 779-788.
[39] J. Redmon and A. Farhadi, "YOLOv3: An Incremental Improvement," arXiv e-prints, 2018.
[40] Dong, Xudong, S. Yan, and C. Duan, "A lightweight vehicles detection network model based on YOLOv5," Engineering Applications of Artificial Intelligence: The International Journal of Intelligent Real-Time Automation 113-(2022):113.
[41] Zhao Y H, Han X, Liu P. “A RPCA and RANSAC based algorithm for ship wake detection in SAR images,” 2018 12th International Symposium on Antennas, Propagation and EM Theory (ISAPE). 2018: 1-4.
[42] Agarwal, Shalove, S. Yadav, and K. Singh, "K-means versus k-means ++ clustering technique." 2012 Students Conference on Engineering and Systems 0.
[43] He K, Jian S, Tang X. Single image haze removal using dark channel prior[C]. IEEE Conference on Computer Vision & Pattern Recognition, 2009.
[44] Chaoyun, Xiao, and Z. Weixing, "Threshold Selection Algorithm for Image Segmentation Based on Otsu Rule and Image Entropy," Computer Engineering (2007).
[45] Yu, Meng Ying, M. L. Han, and C. Y. Shee, "Autofocusing algorithm comparison in bright field microscopy for automatic vision aided cell micromanipulation." IEEE International Conference on Nano/molecular Medicine & Engineering IEEE, 2010.
[46] Jain, Anil K., and Farshid Farrokhnia. "Unsupervised Texture Segmentation Using Gabor Filters." Pattern Recognition 24, no. 12 (January 1991): 1167–86.
[47] Kawata, Satoshi, and Y. Ichioka, "Iterative image restoration for linearly degraded images. II. Reblurring procedure," Journal of the Optical Society of America 70.7(1980):768-772.
[48] Zhou, W., A. C. Bovik, H. R. Sheikh, and E. P. Simoncelli. "Image Quality Assessment: From Error Visibility to Structural Similarity." IEEE Transactions on Image Processing. Vol. 13, Issue 4, April 2004, pp. 600–612.
[49] Rodriguez, Robert N. “A guide to the Burr type XII distributions.” Biometrika, Vol. 64, Number 1, 1977, pp. 129–134.
[50] X. Sun, Y. Liu, Z. Yan, P. Wang, W. Diao, and K. Fu, “SRAFNet: Shape robust anchor-free network for garbage dumps in remote sensing imagery,” IEEE Trans. Geosci. Remote Sens., vol. 59, no. 7, pp. 6154–6168, Jul. 2021.
[51] Shao, Quanxi, "Notes on maximum likelihood estimation for the three-parameter Burr XII distribution." Computational Statistics & Data Analysis 45.3(2004):675-687.
[52] M. Ester, H. P. Kriegel, J. Sander, and X. Xu, "A Density-Based Algorithm for Discovering Clusters in Large Spatial Databases with Noise," AAAI Press, 1996.
[53] Q. He, X. Sun, Z. Yan, B. Li and K. Fu, "Multi-Object Tracking in Satellite Videos with Graph-Based Multitask Modeling," in IEEE Transactions on Geoscience and Remote Sensing, vol. 60, pp. 1-13, 2022.
[54] Gupta, V., Rahmani, M.K.I. IoT-based nano wireless sensor approach for detection of ships using convolutional neural network https://doi.org/10.1007/s11760-024-03460-2, Springer Nature, SCIE Fay, Michael P., and E. J. Feuer, "Confidence intervals for directly standardized rates: a method based on the gamma distribution. " Statistics in Medicine 16.7(2010):791-801.
[55] V. Gupta, N. Marriwala and M. Gupta, "A GUI based application for Low Intensity Object Classification & Count using SVMApproach,"2021 6thInternational Conference on Signal Processing, Computing and Control (ISPCC), 2021, pp. 299-302, doi: 10.1109/ISPCC53510.2021.9609470. IEEE.